ZnO-nanotaper array sacrificial templated synthesis of noble-metal building-block assembled nanotube arrays as 3D SERS-substrates

ARTICLE *in* NANO RESEARCH · MARCH 2015

Impact Factor: 7.01 · DOI: 10.1007/s12274-014-0577-x

8 AUTHORS, INCLUDING:

Chuhong Zhu
Chinese Academy of Sciences
28 PUBLICATIONS **449** CITATIONS
SEE PROFILE

Qing Huang
Chinese Academy of Sciences
100 PUBLICATIONS **1,478** CITATIONS
SEE PROFILE

Haibin Tang
Chinese Academy of Sciences
13 PUBLICATIONS **196** CITATIONS
SEE PROFILE

Nano Research 2015, 8(3): 957–966
DOI 10.1007/s12274-014-0577-x
Research Article
ISSN 1998-0124
CN 11-5974/O4

ZnO-nanotaper array sacrificial templated synthesis of noble-metal building-block assembled nanotube arrays as 3D SERS-substrates

Chuhong Zhu[1], Guowen Meng[1,2] (✉), Qing Huang[3], Xiujuan Wang[1], Yiwu Qian[1], Xiaoye Hu[1], Haibin Tang[1], and Nianqiang Wu[4]

[1] *Key Laboratory of Materials Physics, and Anhui Key Laboratory of Nanomaterials and Nanotechnology, Institute of Solid State Physics, Chinese Academy of Sciences, Hefei 230031, China*
[2] *University of Science and Technology of China, Hefei 230026, China*
[3] *Institute of Technical Biology and Agriculture Engineering, Hefei Institutes of Physical Science, Chinese Academy of Sciences, Hefei 230031, China*
[4] *Department of Mechanical & Aerospace Engineering, West Virginia University, P.O. Box 6106, Morgantown, WV 26506, USA*

Received: 16 April 2014
Revised: 5 September 2014
Accepted: 6 September 2014

KEYWORDS
noble metal nanotube,
hierarchical nanostructure,
SERS,
template synthesis,
ZnO nanotaper

ABSTRACT

This paper describes a ZnO-nanotaper array sacrificial templated synthetic approach for the fabrication of the arrays of nanotubes with tube-walls assembled by building-blocks of Ag-nanoplates, Au-nanorods, Pt-nanothorns or Pd-nanopyramids, thus possessing high-density 3D "hot spots" in sub-10-nm gaps of neighboring building blocks with nano-tips, -corners or -edges. Additionally, these hierarchical nanostructure arrays possess high surface area with rich surface chemistry, being beneficial to capturing the analyte. The Ag-nanoplate-assembled nanotube arrays can be used as sensitive surface-enhanced Raman scattering (SERS) substrates with good signal uniformity and reproducibility. Using such Ag hierarchical nanostructure arrays as SERS-substrates, not only has 10^{-14} M rhodamine 6G been identified, but also 10^{-7} M polychlorinated biphenyls (PCBs, a notorious class of persistent organic pollutants) are recognized, and even two congeners of PCBs can be identified in a mixture, showing the potential applications of the materials in SERS-based rapid detection of environmental organic pollutants.

1 Introduction

Raman scattering signals from molecules adsorbed on nanostructured noble-metal substrates can be enhanced by a factor of a million or even more as compared to those from free molecules in a process known as surface-enhanced Raman scattering (SERS) [1], which offers great opportunities in ultra-trace

Address correspondence to gwmeng@issp.ac.cn

chemical analysis [2–5]. This spectacular enhancement is mainly attributed to the electromagnetic-field enhancement resulting from plasmon-induced extremely large electric fields within the so-called "hot spots" located in the nanoscale gaps [6–9], and around the nanoscale sharp edges [10], corners and tips [11] of the noble- metal substrates. An increase in the number and intensity of hot spots in a large volume will enhance SERS-activity. Therefore, SERS-substrates with high-density 3D "hot spots" have recently attracted intensive interest. For example, vertically aligned Au-nanoparticle-decorated carbon nanotube arrays with high-density 3D "hot spots" can provide highly sensitive SERS signals of target molecules with an ultra-low concentration down to 10 fM [12], and arrays of Ag-nanoisland-decorated glass nanopillars show high average enhancement factors over 10^7 due to the high-density "hot spots" located on both the top and side of the glass nanopillars [13]. Other 3D SERS-substrates, such as Ag-coated carbon nanotube arrays [14], Au–hafnia–carbon nanotube arrays [15], Ag-nanoparticle-decorated ZnO nanotaper arrays [16], Au-coated TiO_2 nanotube arrays [17], and Au-capped Si nanowire/nanopillar arrays [18, 19], also display high SERS-activity owing to their high-density 3D "hot spots". Compared to round-shaped nanoparticles, noble-metal nanostructures with nanoscale corners, edges and/or tips have much stronger capability of concentrating the plasmon-induced electromagnetic field [10, 11, 20, 21]. Therefore, if these unique nanostructures are assembled into SERS-substrates, strong "hot spots" will exist in the gaps between the neighboring building-blocks, thus SERS-substrates with a high density of 3D "hot spots" could be expected.

Herein, we present a general synthetic approach, based on sacrificial ZnO-nanotaper array templated electrodeposition, to fabricate 3D SERS-substrates of vertically aligned noble-metal nanotube arrays with each tube-wall assembled by building-blocks of Ag-nanoplates, Au-nanorods, Pt-nanothorns or Pd-nanopyramids, as shown in Fig. 1. First, vertically aligned ZnO-nanotaper arrays are electrodeposited on an indium tin oxide (ITO) substrate in $Zn(NH_3)_4(NO_3)_2$ aqueous solution using graphite as working electrode (Step 1 in Fig. 1) [16]. Subsequently,

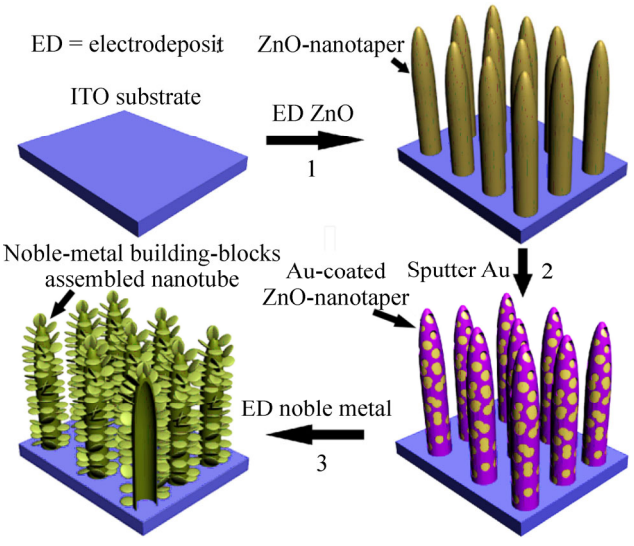

Figure 1 Schematic for the synthesis of noble-metal building-block assembled nanotube arrays. (1) Vertically aligned ZnO-nanotaper arrays are electrodeposited on an ITO substrate. (2) Au-nanoparticles are sputtered on ZnO-nanotapers. (3) Noble-metal building-blocks are assembled on ZnO-nanotapers via electrodeposition, meanwhile the ZnO-nanotapers are etched by citric acid in the electrolyte, and noble-metal building-block assembled top-end-closed nanotube arrays are achieved.

Au-nanoparticles are sputtered onto the ZnO-nanotapers to provide nucleation sites for metal building-blocks to grow (Step 2 in Fig. 1). Next, metal building-blocks are assembled on the Au-nanoparticle-decorated ZnO-nanotapers via electrodeposition in metal ions and citric acid electrolyte where the electrodeposited metal grow into Ag-nanoplates [22], Au-nanorods, Pt-nanothorns or Pd-nanopyramids under the guidance of citric acid. In the mean time the ZnO-nanotapers themselves are gradually eroded by citric acid in the electrolyte. As a result, arrays of top-end-closed nanotubes assembled by noble-metal building-blocks are achieved (Step 3 in Fig. 1). Besides high surface area, rich surface chemistry and anti-agglomeration, the arrays of noble-metal building-block assembled top-end-closed nanotubes have the following additional advantages. First, highly concentrated electromagnetic fields are generated near the nanoscale corners, edges and tips of individual building-blocks, creating strong hot spots in the nano-gaps between these neighboring nanostructures. Therefore such noble-metal nanotube arrays should possess a high density of 3D "hot spots" and can serve as sensitive SERS-substrates. Second, the noble-metal building-block assembled nanotube arrays

are chemically stable in both acidic and alkaline solutions, allowing their applications in a wide range of environment. Third, the arrays of noble-metal building-block assembled nanotubes with low density and high surface area have lower cost than that of the conventional compact noble-metal nanostructures [23]. Using the arrays of Ag-nanoplate-assembled nanotubes as sensitive SERS-substrate, not only laboratory probe molecules of rhodamine 6G (R6G) with a low concentration of 10^{-14} M can be identified, but also 10^{-7} M polychlorinated biphenyls (PCBs, a notorious class of persistent organic pollutants) can be recognized, and even two congeners of PCBs can be identified in a mixture, showing the promising potential applications of the materials in SERS-based rapid detection of trace-level environmental organic pollutants.

2 Experimental

2.1 Electrodeposition of ZnO-nanotaper arrays

ZnO-nanotaper arrays were electrodeposited on an ITO substrate (0.5 cm × 3 cm) with a graphite sheet as anode at a constant current density (0.7 mA·cm^{-2}) for 2.5 h in $Zn(NH_3)_4(NO_3)_2$ aqueous solution (100 mL, 0.1 M), which was prepared by gradually dropping aqueous ammonia into zinc nitrate hexahydrate aqueous solution until the solution became clear. The electrochemical cell was put into a water bath at 80 °C during the whole electrodeposition. Finally, the ITO substrate was cleaned with de-ionized water and dried with high-purity flowing nitrogen gas.

2.2 Sputtering Au on ZnO-nanotaper arrays

Au was sputtered on the ZnO-nanotapers using a K550X sputter coater with an electric current of 10 mA for 8 min.

2.3 Electrodeposition of Ag-nanoplate-assembled nanotube arrays

Ag was electrodeposited on the Au-coated ZnO-nanotaper arrays with a graphite sheet as anode under a constant current density (80 μA·cm^{-2}) for 20 min in an aqueous solution (100 mL) containing $AgNO_3$ (2.0 g·L^{-1}) and citric acid (12 g·L^{-1}). Then, the substrate was cleaned with de-ionized water and dried with high-purity flowing nitrogen gas.

2.4 Electrodeposition of Pt-nanothorn-assembled nanotube arrays

Pt-nanothorns were electrodeposited on the Au-coated ZnO-nanotaper arrays under a constant current density (350 μA·cm^{-2}) for 30 min in an aqueous solution (100 mL) containing $H_2PtCl_6{\cdot}6H_2O$ (2.0 g·L^{-1}) and citric acid (8.4 g·L^{-1}). Then, the substrate was cleaned with de-ionized water and dried with high-purity flowing nitrogen gas.

2.5 Electrodeposition of Au-nanorod-assembled nanotube arrays

Au-nanorods were electrodeposited on the Au-coated ZnO-nanotaper arrays under a constant current density (80 μA·cm^{-2}) for 60 min in an aqueous solution (100 mL) containing $AuCl_3{\cdot}HCl{\cdot}4H_2O$ (0.8 g·L^{-1}) and citric acid (8.0 g·L^{-1}). Then, the substrate was cleaned with de-ionized water and dried with high-purity flowing nitrogen gas.

2.6 Electrodeposition of Pd-nanopyramid-assembled nanotube arrays

Pd-nanopyramids were electrodeposited on the Au-coated ZnO-nanotaper arrays under a constant current density (300 μA·cm^{-2}) for 30 min in an aqueous solution (100 mL) containing Na_2PdCl_4 (2.0 g·L^{-1}) and citric acid (9.0 g·L^{-1}). Then, the substrate was cleaned with de-ionized water and dried with high-purity flowing nitrogen gas.

2.7 Modification of mono-6-thio-β-cyclodextrin onto SERS-substrates

The as-prepared SERS-substrates (0.3 cm × 0.2 cm) were immersed in 1 mL of 0.1 mM mono-6-thio-β-cyclodextrin (HS-β-CD) in a *N*,*N*-dimethylformamide (DMF) solution for 12 h for chemical modification. After being modified with HS-β-CD, the SERS-substrates were taken out, rinsed with DMF, and dried in high-purity Ar. Then HS-β-CD-modified SERS-substrates were immersed in 1 mL of 3 × 10^{-5}, and 10^{-7} M 3,3′,4,4′-tetrachlorobiphenyl (PCB-77, one congener of PCBs) acetone solutions for 4 h, then taken

out, rinsed with acetone, and dried in a laboratory fume cupboard.

2.8 SERS measurements

The as-prepared Ag-nanoplate-assembled nanotube arrays were cleaned by plasma (PDC-32G) for 15 min to remove the citric acid adsorbed on the surfaces, and then used as SERS-substrates. SERS measurements were conducted under a confocal microprobe Raman system (Renishaw, inVia) with an excitation wavelength of 532 nm. During SERS measurements, the laser light was vertically projected onto the samples with a beam diameter of ~5 μm. For checking their SERS signal uniformity, the substrates (0.3 cm × 0.2 cm) were immersed in 10 mL of R6G aqueous solutions (10^{-6} M) for 4 h, then taken out and dried with high-purity flowing nitrogen immediately. To show its SERS sensitivity, the SERS-substrates (0.3 cm × 0.2 cm) were immersed in three R6G solutions (20 mL) with low concentrations of 10^{-8}, 10^{-10} and 10^{-14} M for 6 h, then taken out and dried with high-purity flowing nitrogen. For enhancement factor (EF) calculations, SERS-substrates were immersed in a 10^{-4} M ethanol solution of 2-naphthalenethiol (2-NT) for 12 h, then taken out, rinsed with ethanol, and dried with high-purity flowing nitrogen. For PCB detection, 10 μL of 3×10^{-4}, 3×10^{-5} and 3×10^{-6} M PCB-77 in n-hexane solutions were dispersed onto SERS-substrates (0.3 cm × 0.2 cm), and dried in a laboratory fume cupboard.

3 Results and discussion

Figure 2(a) shows a scanning electron microscopy (SEM) image of the vertically aligned ZnO-nanotaper arrays electrodeposited on the ITO-substrate, with an average nanotaper middle diameter about 400 nm and length of 3.5 μm (also see Fig. S1(a) in the Electronic Supplementary Material (ESM)). After top-view ion-sputtering with Au, Au-nanoparticles were decorated on the ZnO-nanotapers (Fig. 2(b)) as nucleation sites for the metal building-blocks to grow. After electrodepositing Ag on the Au-nanoparticle-decorated ZnO-nanotapers in $AgNO_3$ and citric acid mixed electrolyte, Ag-nanoplates were assembled onto the surface of the ZnO-nanotapers while the ZnO-nanotapers were gradually dissolved, forming arrays of vertically aligned Ag-nanoplates-assembled top-end-closed nanotubes with an average diameter about 500 nm (Fig. 2(c)). Close-up SEM observation (Fig. 2(d)) reveals that the thickness of the serrated Ag-nanoplate building-blocks is about 16 nm, with lengths ranging from tens of nm to 250 nm. SEM (Fig. 2(e)) and transmission electron microscopy (TEM) (Fig. S1(b) in the ESM) observations on the broken nanotubes display their hollow tubular geometrical features, giving evidence of the sacrificial ZnO-nanotaper dissolution. Moreover, energy dispersive X-ray spectroscopy (EDS) (Fig. 2(f)) reveals that the resulting nanotubes were mainly composed of Ag with a small amount of Au that once served as nucleation sites for Ag-nanoplates to grow. The absence of Zn and O in the EDS spectrum further confirms the dissolution of the sacrificial ZnO-nanotapers by citric acid etching, being similar to that of ZnO-nanowires used as sacrificial templates for the synthesis of multimetallic alloy nanotubes [24].

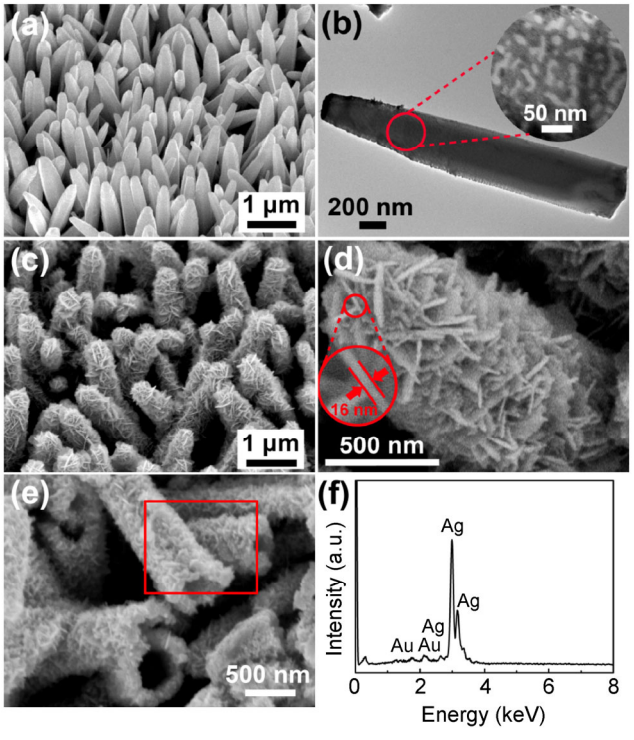

Figure 2 (a) SEM image of the ZnO-nanotaper arrays. (b) TEM images of a single Au-nanoparticle-decorated ZnO-nanotaper. (c) SEM image of the top-end-closed Ag-nanoplate-assembled nanotube arrays. (d) A close-up SEM view of the surface of the Ag-nanoplate-assembled nanotube. (e) SEM view of the broken Ag-nanoplate-assembled nanotubes. (f) EDS spectrum taken from the red box shown in (e).

The Ag-nanoplate-assembled nanotube arrays have nanoscale edges, corners and gaps (Fig. S2 in the ESM), and hence can create a highly concentrated electromagnetic field. Consequently, the arrays of Ag-nanoplate-assembled top-end-closed nanotubes possess high-density 3D "hot spots" due to strong coupling of such high-intensity plasmonic fields.

In addition to Ag, arrays of other noble-metal building-block assembled nanotubes can also be achieved by using their metal ions in the electrolyte for the electrodeposition assembling on the sacrificial ZnO-nanotapers. For example, arrays of top-end-closed nanotubes assembled by Pt-nanothorns (Figs. 3(a)–3(c)), Au-nanorods (Figs. 3(d)–3(f)) and Pd-nanopyramids (Figs. 3(g)–3(i)) have been fabricated. As the building-blocks of Ag-nanoplates, Pt-nanothorns, Au-nanorods and Pd-nanopyramids, have nanoscale sharp tips, corners and/or edges, hence individual building-blocks can create highly concentrated electromagnetic fields. Consequently, the arrays of noble-metal building-block assembled top-end-closed nanotubes possess high-density 3D "hot spots" due to strong coupling of such high-intensity plasmonic fields. Therefore, the arrays of noble-metal building-block assembled nanotubes should exhibit high SERS-activity due to their high-density 3D SERS "hot spots" and high surface area.

Ag generally exhibits the most effective SERS among all noble metals when illuminated by a visible laser [25–27], therefore the Ag-nanoplate-assembled nanotube arrays are taken as the example to demonstrate their high-density 3D SERS "hot spots", high SERS-activity and good SERS-signal uniformity. The UV–Visible spectrum of the Ag-nanoplate-assembled nanotubes reveals strong plasmon absorption from 390 to 550 nm with an absorption band peak

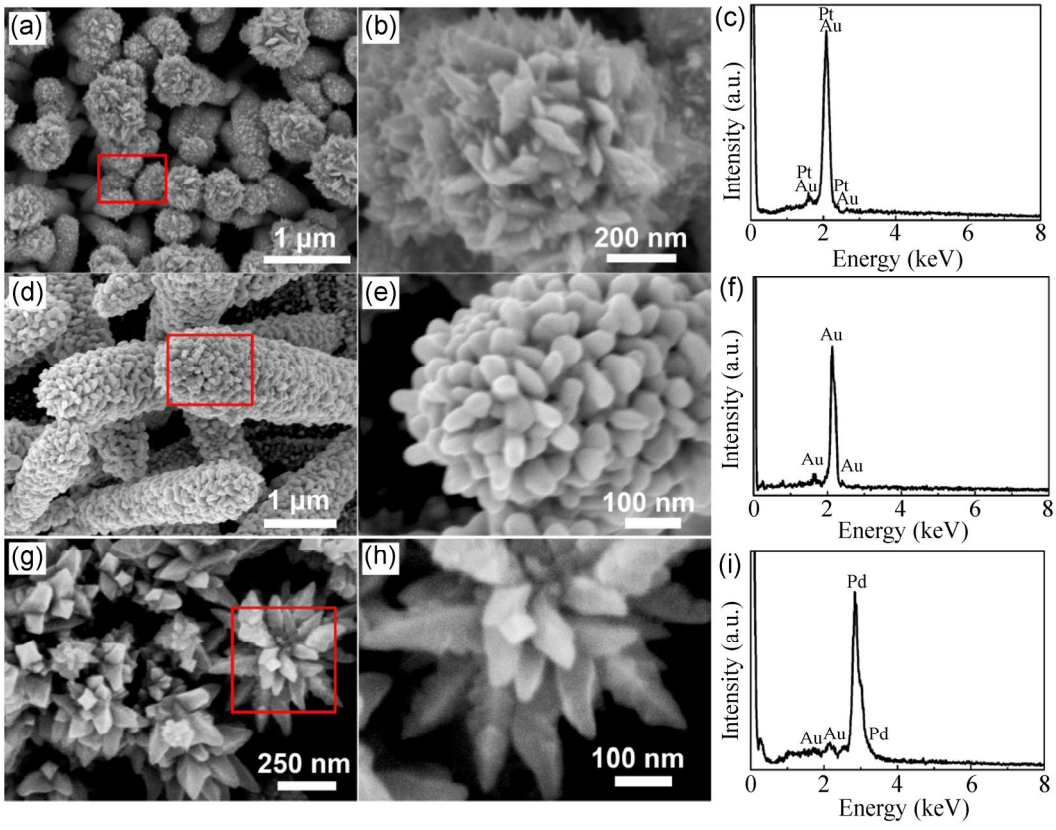

Figure 3 (a) and (b) SEM images of the as-prepared arrays of vertically aligned Pt-nanothorn-assembled top-end-closed nanotubes with different magnifications, and (c) EDS spectrum taken from the area in the red box marked in the inset of (a). (d) and (e) SEM observation of the as-prepared arrays of vertically aligned Au-nanorod-assembled nanotubes with different magnifications, and (f) EDS spectrum taken from the area in the red box marked in the inset of (d). (g) and (h) SEM observation of the as-prepared arrays of vertically aligned Pd-nanopyramid-assembled nanotube nanotubes with different magnifications, and (i) EDS spectrum taken from the area in the red box marked in the inset of (g).

centered at 475 nm (Fig. 4(a)), indicating that the Ag-nanoplate-assembled nanotubes can generate high electromagnetic enhancement of Raman signals when the excitation laser with a wavelength of 532 nm was used in Raman measurements. Then, using a finite element method [28], we tried to demonstrate that the nanoscale gaps between Ag nanostructures can generate SERS "hot spots". For simplification, we consider a pair of neighboring Ag-nanoplate-assembled nanotubes as shown in the upper panel of Fig. 4(b). The simulation result (lower panel in Fig. 4(b)) confirms that there indeed exist "hot spots" as indicated by

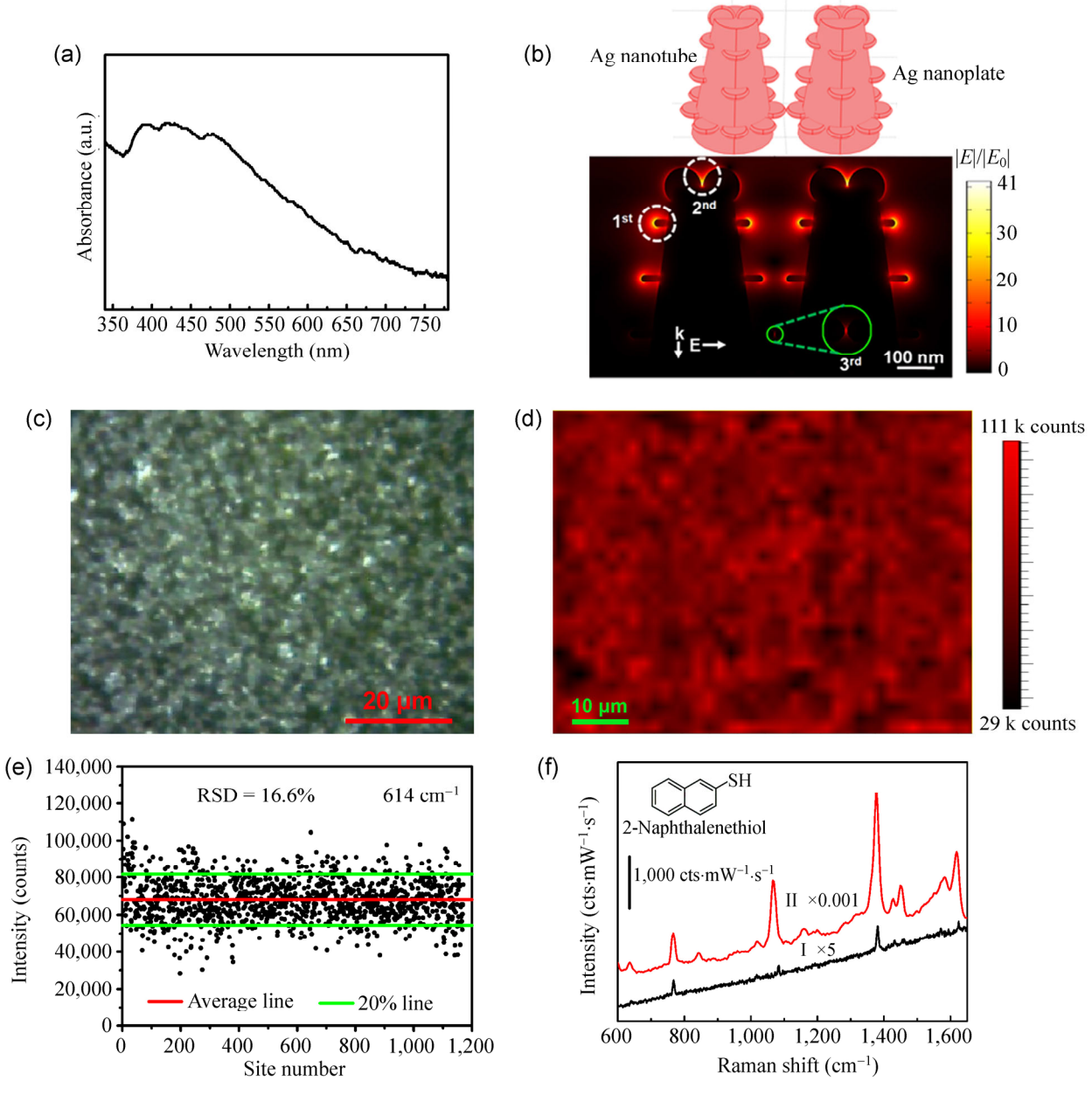

Figure 4 (a) Optical absorbance spectrum of the Ag-nanoplate assembled nanotube arrays. (b) Simplified two neighboring Ag-nanoplate-assembled nanotubes (upper panel) and the calculated electric field distribution (lower panel) at the excitation wavelength of 532 nm. (c) Optical image of Ag nanoplate-assembled nanotube arrays. (d) SERS mapping of the area shown in (c). (e) The SERS intensity deviation of 10^{-6} M R6G calculated by using the spectra from the SERS mapping shown in (d). (f) (Curve I) normal Raman spectrum of a 2-NT film, and (curve II) SERS spectrum of a monolayer 2-NT on the Ag-nanoplate-assembled nanotubes.

the circles and marked with 1st (around nanoplate edges), 2nd (in the nanoscale gaps between neighboring nanoplates on a nanotube) and 3rd (in the nanoscale gaps between neighboring nanoplates grown on two neighboring nanotubes), respectively.

To optimize the size of the Ag-nanoplates on nanotubes for higher SERS-activity, the SERS performance of the samples fabricated by different electrodeposition durations were compared by using R6G as a probe molecule. With an increase of electrodeposition duration from 8 to 20 min, the Ag nanoplates on nanotubes became larger and denser (Figs. S3(a)–S3(e) in the ESM), and their SERS-activities were significantly improved (Fig. S3(f) in the ESM). Further prolonging the electrodeposition duration weakened the intensity of SERS peaks (Fig. S3(f) in the ESM), because very large Ag nanoplates led to the surface contact of neighboring nanotubes and thus reduced the specific surface area of nanotubes illuminated by the laser beam. SERS measurements on the other noble metal nanostructure-assembled nanotube arrays (Fig. S4 in the ESM) further confirmed that the SERS-activity of Ag nanoplate-assembled nanotubes was higher than that of the others, while the Pt nanothorn-assembled nanotubes exhibited the lowest SERS-activity.

Then we examined the SERS-signal uniformity of the Ag-nanoplate-assembled nanotube arrays. Figure 4(d) shows the SERS mapping of 10^{-6} M R6G taken from a 60 μm × 75 μm area (Fig. 4(c)). The calculated relative standard deviation (RSD) of the intensities of the peaks at 614 cm^{-1} was 16.6% (Fig. 4(e)), revealing the good signal reproducibility and uniformity of the Ag hierarchical nanostructure arrays [29]. To further check the SERS-activity of the Ag hierarchical nanostructure arrays, the EF was calculated by comparing the peak intensities of the 2-NT SERS spectrum (curve II in Fig. 4(f)) to the corresponding normal Raman spectrum (curve I in Fig. 4(e)) from a 2-NT film, using the formula reported elsewhere [30, 31]. The average EF was estimated to be 8.3×10^7 (see the details in the ESM), approaching the requirement for single molecule detection [6]. The SERS spectra of R6G with different concentrations adsorbed on the Ag hierarchical nanostructure arrays are shown in Fig. 5(a). The characteristic bands of R6G were distinctly observed

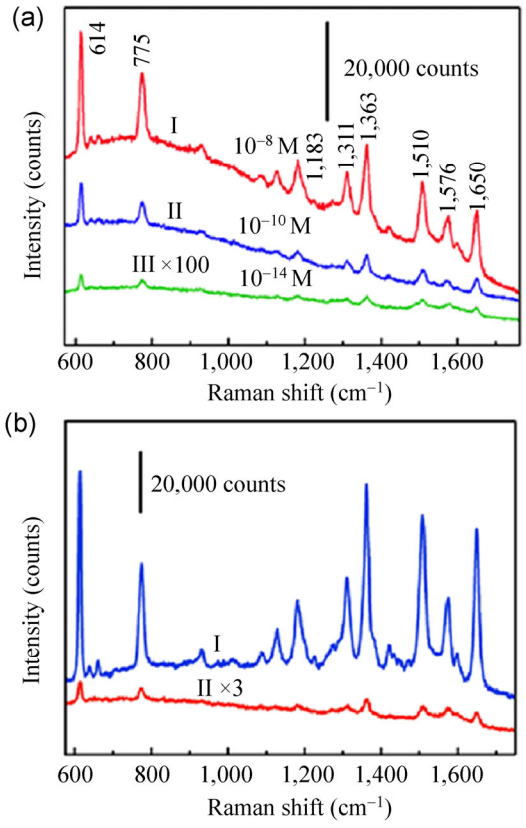

Figure 5 (a) SERS spectra of (curve I) 10^{-8}, (curve 2) 10^{-10} and (curve 3) 10^{-14} M R6G probed by using the Ag hierarchical nanostructure arrays, acquisition time: 20 s. (b) SERS spectra of 10^{-6} M R6G probed using (curve I) Ag-nanoplate-assembled nanotube arrays and (curve II) Ag-nanoplate-assembled film, respectively. Acquisition time: 5 s.

even with a concentration as low as 10^{-14} M, revealing that the Ag hierarchical nanostructure arrays can serve as sensitive SERS-substrates.

Next, to demonstrate that the 3D SERS-substrate is more sensitive than a two-dimensional (2D) SERS-substrate that consists of the same or similar building-blocks, we compared SERS signals from these two kinds of substrates. It was found that the intensity of the SERS signal from the Ag-nanoplate-assembled nanotube arrays (with a total surface area of Ag-nanoplates ~20 cm^2 on a 1 cm^2 ITO substrate) was about 30 times higher (curve I in Fig. 5(b)) than that (curve II in Fig. 5(b)) from the Ag-nanoplate-assembled film (with a total surface area of Ag-nanoplates ~4 cm^2 on a 1 cm^2 ITO substrate, see Fig. S5 in the ESM for its morphology). This result indicates that the Ag-nanoplate-assembled 3D SERS-substrate has significantly higher SERS-activity than that of the

Ag-nanoplate-assembled 2D SERS-substrate due to its higher surface area and larger number of "hot spots". Then we also compared the SERS activity of the Ag-nanoplate-assembled nanotube arrays with that of the film assembled by Ag nanoparticles with an average diameter of about 70 nm (Fig. S6(a) in the ESM). The Ag-nanoplate-assembled nanotube arrays exhibit SERS peaks (curve I in Fig. 5(b)) with intensities about seven times higher than those of the Ag-nanoparticle-assembled film (Fig. S6(b) in the ESM), further demonstrating that our Ag-nanoplate-assembled nanotube arrays can be used as sensitive SERS-substrates.

To demonstrate a potential application of the as-prepared 3D SERS-substrate, we examined the SERS-sensitivity of the Ag hierarchical nanostructure arrays to PCBs, one notorious class of persistent organic pollutants defined in the Stockholm Convention [32]. Curves I–III in Fig. 6(a) show the SERS spectra of PCB-77 (one congener of PCBs) with different concentrations on the bare Ag hierarchical nanostructure arrays. There are seven distinct bands at 584, 677, 1,032, 1,137, 1,245, 1,299 and 1,598 cm^{-1} in the SERS spectra, corresponding well with the reported results [33, 34]. It is not easy for PCBs molecules to adsorb onto bare Ag [35], but a single PCB molecule can be included into the hydrophobic cavity of β-cyclodextrin (β-CD) [36], and therefore the Ag hierarchical nanostructure arrays were modified with HS-β-CD to effectively capture PCBs for more sensitive SERS-based detection. As expected, there exist weak SERS signals of HS-β-CD from the HS-β-CD-modified Ag hierarchical nanostructure arrays (Fig. S7 in the ESM) [37]. Curves IV and V in Fig. 6(a) show the SERS spectra of PCB-77 adsorbed on the HS-β-CD-modified Ag hierarchical nanostructure arrays. A comparison of curve IV with III reveals that the SERS spectrum of PCB-77 is much more distinctive after HS-β-CD modification. When the PCB-77 concentration was reduced to 10^{-7} M, the bands at 1,032, 1,245, 1,299, and 1,598 cm^{-1} (curve V in Fig. 6(a)) can still be identified. To show the ability of the material to distinguish between different congeners of PCBs in mixed solutions, we tried to identify 2-chlorobiphenyl (PCB-1) and PCB-77 in their mixed solution. Figure 6(b) shows the SERS spectra of a mixed solution of PCB-77 and PCB-1 (curve I), and a pure solution of PCB-1 (curve II). Although many characteristic peaks (e. g., 679, 1,034, 1,246, 1,300 and 1,600 cm^{-1}) are similar, the peaks at 965, 998 and 1,615 cm^{-1} assigned to PCB-1 and those at 584 and 1,137 cm^{-1} assigned to PCB-77 can be clearly distinguished in the spectrum of the mixture (curve I). Therefore, the HS-β-CD-modified Ag hierarchical nanostructure arrays can serve as effective SERS-substrates for identifying different congeners of PCBs in mixed solutions.

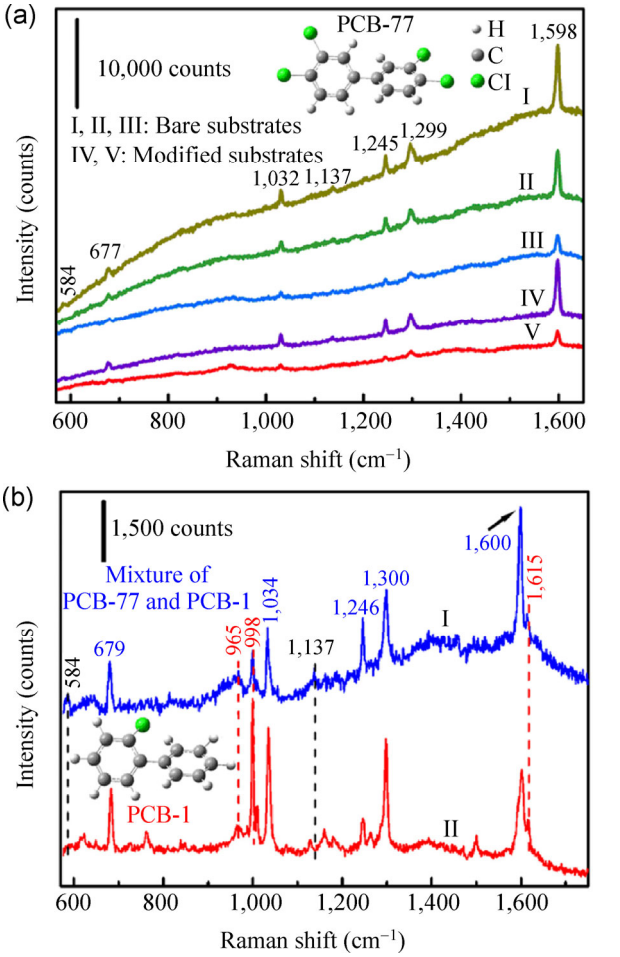

Figure 6 SERS sensitivity to PCBs. (a) SERS spectra of (curve I) 3×10^{-4}, (curve II) 10^{-4} and (curve III) 3×10^{-5} M PCB-77 probed using the bare Ag hierarchical nanostructure arrays, and (curve IV) 3×10^{-5} and (curve V) 1×10^{-7} M PCB-77 probed by using the HS-β-CD-modified substrates. Acquisition time: 30 s. (b) SERS spectra of 2×10^{-5} M PCB-77 and 1×10^{-5} M PCB-1 mixed solution (curve I), and a 3×10^{-5} M PCB-1 solution (curve II) probed using the HS-β-CD-modified Ag hierarchical nanostructure arrays. Acquisition time: 10 s.

4 Conclusions

A ZnO-nanotaper array sacrificial template-based electrodeposition approach has been developed to fabricate arrays of top-end-closed noble-metal nanotubes with the tube-walls consisting of building-blocks of Ag-nanoplates, Au-nanorods, Pt-nanothorns, or Pd-nanopyramids. The hierarchical noble-metal nanostructure arrays possess high surface area and high-density 3D SERS "hot spots". As the high surface area enables easy adsorption of the analyte molecules, and the high-density 3D "hot spots" ensure the adequate excitation of SERS signals of the adsorbed molecules, the hierarchical noble-metal nanostructure arrays can serve as sensitive SERS-substrates. The arrays of Ag hierarchical nanostructures, as sensitive SERS-substrates with good signal uniformity and reproducibility, demonstrate promising potential in identifying trace-level organic pollutants such as PCBs. Therefore, these hierarchical noble-metal nanostructure arrays are expected to be employed as highly sensitive 3D SERS-substrates for chemical and biological sensing applications.

Acknowledgements

This work was financially supported by the National Basic Research Program of China (No. 2013CB934304), the CAS/SAFEA International Partnership Program for Creative Research Teams, and the National Natural Science Foundation of China (Nos. 21201168, 11274312, 61006068 and 51101151). N. Q. W. is grateful for the partial support by NSF (No. EPS 1003907).

Electronic Supplementary Material: Supplementary material (calculation of SERS enhancement factor, SEM images and SERS spectra) is available in the online version of this article at http://dx.doi.org/10.1007/s12274-014-0577-x.

References

[1] Jeanmaire, D. L.; Van Duyne, R. P. Surface Raman spectroelectrochemistry: Part I. Heterocyclic, aromatic, and aliphatic amines adsorbed on the anodized silver electrode. *J. Electroanal. Chem. Interfacial Electrochem.* **1977**, *84*, 1–20.

[2] Haynes, C. L.; Yonzon, C. R.; Zhang, X. Y.; Van Duyne, R. P. Surface-enhanced Raman sensors: Early history and the development of sensors for quantitative biowarfare agent and glucose detection. *J. Raman Spectrosc.* **2005**, *36*, 471–484.

[3] Cecchini, M. P.; Turek, V. A.; Paget, J.; Kornyshev, A. A.; Edel, J. B. Self-assembled nanoparticle arrays for multiphase trace analyte detection. *Nat. Mater.* **2012**, *12*, 165–171.

[4] Li, J. F.; Huang, Y. F.; Ding, Y.; Yang, Z. L.; Li, S. B.; Zhou, X. S.; Fan, F. R.; Zhang, W.; Zhou, Z. Y.; Wu, D. Y. et al. Shell-isolated nanoparticle-enhanced Raman spectroscopy. *Nature* **2010**, *464*, 392–395.

[5] Anker, J. N.; Hall, W. P.; Lyandres, O.; Shah, N. C.; Zhao, J.; Van Duyne, R. P. Biosensing with plasmonic nanosensors. *Nat. Mater.* **2008**, *7*, 442–453.

[6] Fang, Y.; Seong, N. H.; Dlott, D. D. Measurement of the distribution of site enhancements in surface-enhanced Raman scattering. *Science* **2008**, *321*, 388–392.

[7] Im, H.; Bantz, K. C.; Lee, S. H.; Johnson, T. W.; Haynes, C. L.; Oh, S. H. Self-assembled plasmonic nanoring cavity arrays for SERS and LSPR biosensing. *Adv. Mater.* **2013**, *25*, 2678–2685.

[8] Pedano, M. L.; Li, S. Z.; Schatz, G. C.; Mirkin, C. A. Periodic electric field enhancement along gold rods with nanogaps. *Angew. Chem. Int. Ed.* **2010**, *49*, 78–82.

[9] Hatab, N. A.; Hsueh, C. H.; Gaddis, A. L.; Retterer, S. T.; Li, J. H.; Eres, G.; Zhang, Z. Y.; Gu, B. H. Free-standing optical gold bowtie nanoantenna with variable gap size for enhanced Raman spectroscopy. *Nano Lett.* **2010**, *10*, 4952–4955.

[10] Lu,Y.; Liu, G. L.; Kim, J.; Mejia, Y. X.; Lee, L. P. Nanophotonic crescent moon structures with sharp edge for ultrasensitive biomolecular detection by local electromagnetic field enhancement effect. *Nano Lett.* **2005**, *5*, 119–124.

[11] Fang, J. X.; Du, S. Y.; Lebedkin, S.; Li, Z. Y.; Kruk, R.; Kappes, M.; Hahn, H. Gold mesostructures with tailored surface topography and their self-assembly arrays for surface-enhanced Raman spectroscopy. *Nano Lett.* **2010**, *10*, 5006–5013.

[12] Lee, S.; Hahm, M. G.; Vajtai, R.; Hashim, D. P.; Thurakitseree, T.; Chipara, A. C.; Ajayan, P. M.; Hafner, J. H. Utilizing 3D SERS active volumes in aligned carbon nanotube scaffold substrates. *Adv. Mater.* **2012**, *24*, 5261–5266.

[13] Oh, Y. J.; Jeong, K. H. Glass nanopillar arrays with nanogap-rich silver nanoislands for highly intense surface enhanced Raman scattering. *Adv. Mater.* **2012**, *24*, 2234– 2237.

[14] Dawson, P.; Duenas, J. A.; Boyle, M. G.; Doherty, M. D.; Bell, S. E. J.; Kern, A. M.; Martin, O. J. F.; Teh, A. S.; Teo, K. B. K.; Milne, W. I. Combined antenna and localized plasmon resonance in Raman scattering from random arrays

of silver-coated, vertically aligned multiwalled carbon nanotubes. *Nano Lett.* **2011**, *11*, 365–371.

[15] Altun, A. O.; Youn, S. K.; Yazdani, N.; Bond, T.; Park, H. G. Metal–dielectric–CNT nanowires for femtomolar chemical detection by surface enhanced Raman spectroscopy. *Adv. Mater.* **2013**, *25*, 4431–4436.

[16] Tang, H. B.; Meng, G. W.; Huang, Q.; Zhang, Z.; Huang, Z. L.; Zhu, C. H. Arrays of cone-shaped ZnO nanorods decorated with Ag nanoparticles as 3D surface-enhanced Raman scattering substrates for rapid detection of trace polychlorinated biphenyls. *Adv. Funct. Mater.* **2012**, *22*, 218–224.

[17] Li, X. H.; Chen, G. Y.; Yang, L. B.; Jin, Z.; Liu, J. H. Multifunctional Au-coated TiO_2nanotube arrays as recyclable SERS substrates for multifold organic pollutants detection. *Adv. Funct. Mater.* **2010**, *20*, 2815–2824.

[18] Schmidt, M. S.; Hübner, J.; Boisen, A. Large area fabrication of leaning silicon nanopillars for surface enhanced Raman spectroscopy. *Adv. Mater.* **2012**, *24*, OP11–OP18.

[19] Jeon, H. C.; Heo, C. J.; Lee, S. Y.; Yang, S. M. Hierarchically ordered arrays of noncircular silicon nanowires featured by holographic lithography toward a high-fidelity sensing platform. *Adv. Funct. Mater.* **2012**, *22*, 4268–4274.

[20] Yuan, Q.; Zhang, Y. F.; Chen, Y.; Wang, R. W.; Du, C. L.; Yasun, E.; Tan, W. H. Using silver nanowire antennas to enhance the conversion efficiency of photoresponsive DNA nanomotors. *Proc. Natl. Acad. Sci. USA* **2011**, *108*, 9331–9336.

[21] Lim, D. K.; Jeon, K. S.; Hwang, J. H.; Kim, H.; Kwon, S.; Suh, Y. D.; Nam, J. M. Highly uniform and reproducible surface-enhanced Raman scattering from DNA-tailorable nanoparticles with 1-nm interior gap. *Nat. Nanotechnol.* **2011**, *6*, 452–460.

[22] Zeng, J.; Tao, J.; Li, W. Y.; Grant, J.; Wang, P.; Zhu, Y. M.; Xia, Y. N. A mechanistic study on the formation of silver nanoplates in the presence of silver seeds and citric acid or citrate ions. *Chem. Asian J.* **2011**, *6*, 376–379.

[23] Zhang, G. X.; Sun, S. H.; Cai, M.; Zhang, Y.; Li, R. Y.; Sun, X. L. Porous dendritic platinum nanotubes with extremely high activity and stability for oxygen reduction reaction. *Sci. Rep.* **2013**, *3*, 1526.

[24] Choi, B. S.; Lee, Y. W.; Kang, S. W.; Hong, J. W.; Kim, J.; Park, I.; Han, S. W. Multimetallic alloy nanotubes with nanoporous framework. *ACS Nano* **2012**, *6*, 5659–5667.

[25] Moskovits, M. Surface-enhanced Raman spectroscopy: Abrief retrospective. *J. Raman Spectrosc.* **2005**, *36*, 485–496.

[26] Tian, Z. Q.; Ren, B.; Wu, D. Y. Surface-enhanced Raman scattering: From noble to transition metals and from rough surfaces to ordered nanostructures. *J. Phys. Chem. B* **2002**, *106*, 9463–9483.

[27] Braun, G.; Pavel, I.; Morrill, A. R.; Seferos, D. S.; Bazan, G. C.; Reich, N. O.; Moskovits, M. Chemically patterned microspheres for controlled nanoparticle assembly in the construction of SERS hot spots. *J. Am. Chem. Soc.* **2007**, *129*, 7760–7761.

[28] Alexander, K. D.; Skinner, K.; Zhang, S. P.; Wei, H.; Lopez, R.Tunable SERS in gold nanorod dimers through strain control on an elastomeric substrate. *Nano Lett.* **2010,** *10*, 4488–4493.

[29] Que, R. H.; Shao, M. W.; Zhuo, S. J.; Wen, C. Y.; Wang, S. D.; Lee, S. T. Highly reproducible surface-enhanced Raman scattering on a capillarity-assisted gold nanoparticle assembly. *Adv. Funct. Mater.* **2011**, *21*, 3337–3343.

[30] Zhang, L.; Lang, X. Y.; Hirata, A.; Chen, M. W. Wrinkled nanoporous gold films with ultrahigh surface-enhanced Raman scattering enhancement. *ACS Nano* **2011**, *5*, 4407–4413.

[31] Huang, Z. L.; Meng, G. W.; Huang, Q.; Yang, Y. J.; Zhu, C. H.; Tang, C. L. Improved SERS performance from Au nanopillar arrays by abridging the pillar tip spacing by Ag sputtering. *Adv. Mater.* **2010**, *22*, 4136–4139.

[32] UNEP. *UNEP 2007 Annual Report* [Online]; UNEP: Nairobi, Kenya, 2008; pp 90–103. http://www.unep.org/PDF/AnnualReport/2007/AnnualReport2007_en_web.pdf (accessed April 16, 2014).

[33] Hu, X. Y.; Meng, G. W.; Huang, Q.; Xu, W.; Han, F. M.; Sun, K. X.; Xu, Q. L.; Wang, Z. M. Large-scale homogeneously distributed Ag-NPs with sub-10 nm gaps assembled on a twolayered honeycomb-like TiO_2 film as sensitive and reproducible SERS substrates. *Nanotechnology* **2012**, *23*, 385705.

[34] Zhu, C. H.; Meng, G. W.; Huang, Q.; Zhang, Z.; Xu, Q. L.; Liu, G. Q.; Huang, Z. L.; Chu, Z. Q. Ag nanosheet-assembled micro-hemispheres as effective SERS substrates. *Chem. Commun*. **2011**, *47*, 2709–2711.

[35] Bantz, K. C.; Haynes, C. L. Surface-enhanced Raman scattering detection and discrimination of polychlorinated biphenyls. *Vib. Spectrosc*. **2009**, *50*, 29–35.

[36] Liu, P.; Zhang, D. J.; Zhan, J. H. Investigation on the inclusions of PCB52 with cyclodextrins by performing DFT calculations and molecular dynamics simulations. *J. Phys. Chem. A* **2010**, *114*, 13122–13128.

[37] Yuan, J. P.; Lai, Y. C.; Duan, J. L.; Zhao, Q. Q.; Zhan, J. H. Synthesis of a β-cyclodextrin-modified Ag film by the galvanic displacement on copper foil for SERS detection of PCBs. *J. Colloid Interface Sci*. **2012**, *365*, 122–126.